Journal of Applied Remote Sensing

RemoteSensing.SPIEDigitalLibrary.org

Hybrid wireless sensor network for rescue site monitoring after earthquake

Rui Wang
Shuo Wang
Chong Tang
Xiaoguang Zhao
Weijian Hu
Min Tan
Bowei Gao

SPIE.

Rui Wang, Shuo Wang, Chong Tang, Xiaoguang Zhao, Weijian Hu, Min Tan, Bowei Gao, "Hybrid wireless sensor network for rescue site monitoring after earthquake," J. Appl. Remote Sens. 10(3), 036020 (2016), doi: 10.1117/1.JRS.10.036020.

Hybrid wireless sensor network for rescue site monitoring after earthquake

Rui Wang,[a,b] Shuo Wang,[a,*] Chong Tang,[a,b] Xiaoguang Zhao,[a] Weijian Hu,[c] Min Tan,[a] and Bowei Gao[c]

[a]Institute of Automation, Chinese Academy of Sciences, State Key Laboratory of Management and Control for Complex Systems, 95 Zhongguancun East Road, Haidian District, Beijing 100190, China

[b]University of Chinese Academy of Sciences, No. 19 Yuquan Road, Shijingshan District, Beijing 100049, China

[c]National Earthquake Response Support Service, No. 1 Yuquan West Street, Shijingshan District, Beijing 100049, China

Abstract. This paper addresses the design of a low-cost, low-complexity, and rapidly deployable wireless sensor network (WSN) for rescue site monitoring after earthquakes. The system structure of the hybrid WSN is described. Specifically, the proposed hybrid WSN consists of two kinds of wireless nodes, i.e., the monitor node and the sensor node. Then the mechanism and the system configuration of the wireless nodes are detailed. A transmission control protocol (TCP)-based request-response scheme is proposed to allow several monitor nodes to communicate with the monitoring center. UDP-based image transmission algorithms with fast recovery have been developed to meet the requirements of in-time delivery of on-site monitor images. In addition, the monitor node contains a ZigBee module that used to communicate with the sensor nodes, which are designed with small dimensions to monitor the environment by sensing different physical properties in narrow spaces. By building a WSN using these wireless nodes, the monitoring center can display real-time monitor images of the monitoring area and visualize all collected sensor data on geographic information systems. In the end, field experiments were performed at the Training Base of Emergency Seismic Rescue Troops of China and the experimental results demonstrate the feasibility and effectiveness of the monitor system. [DOI: 10.1117/1.JRS.10.036020]

Keywords: wireless sensor network; earthquake disaster; environment monitoring; monitor node; sensor node; image transmission.

Paper 16187 received Mar. 10, 2016; accepted for publication Aug. 2, 2016; published online Aug. 25, 2016.

1 Introduction

The first 24 h after earthquake disasters are the most critical for the survival of victims.[1,2] Unfortunately, this is also the time period when the fewest resources are available to the rescuers.[3] In addition, rescuers engaged in search and rescue activities for retrieving victims from collapsed buildings at the disaster site are at high risk of additional injuries due to potential safety issues such as landslides, falling rocks, aftershocks, and so forth.[4,5] A low-complexity, rapidly deployable, and real-time monitor system would allow the guarantee of rapid emergency responses, and sensibly reduce the adverse effects by providing immediate monitor images and sensor data of the hazardous areas and making this information available to the rescuers.[6–9]

Traditional wired monitor systems face the challenges of deployment and maintenance due to the complicated geographical conditions and to the limited power supply in disaster-hit areas.[10] Some satellite remote sensing systems are used to assess risks due to earthquakes, volcanoes, floods, and so on, and provide critical information for decision support by emergency

*Address all correspondence to: Shuo Wang, E-mail: shuo.wang@ia.ac.cn

1931-3195/2016/$25.00 © 2016 SPIE

managers.[11–14] Schmidt developed a method to map and monitor aquatic surface-growing weeds in a river using satellite imagery.[12] The Food and Agriculture Organization of the United Nations utilized satellite remote sensing data to monitor vegetation and rainfall developments over large areas.[13] Remarkably, wireless sensor networks (WSNs) have been successfully utilized for environment monitoring of areas which are at high risk of geological, environmental, or other disasters.[15–20] Pogkas et al. presented an ad-hoc sensor network developed for a disaster relief application that helps rescue teams collect information about the presence of people in a collapsed building space and the state of the ruins.[18] Ohbayashi et al. designed an autonomous sensing node network to monitor landslide disasters and to transmit urgent data.[19] Huang et al. addressed the design of an agricultural water quality monitoring system based on WSN.[20] Additionally, the concept of employing balloons and unmanned aerial vehicles (UAVs) to acquire imagery for disaster monitoring has progressed into actual implementation in recent years.[21–26] For example, Asahizawa et al. proposed a ballooned wireless network to promptly observe and grasp the information around the disaster area from sky upon the occurrence of disaster.[25] Figueira et al. presented a concept of UAV mission design in geomatics, applied to the generation of thematic maps for a multitude of civilian and military applications.[27]

Although all the above methods have achieved satisfactory performance on surveillance over disaster-hit regions, few methods focus on real-time monitoring of a localized rescue area (say, within a region with a radius of about 200 m). Satellite methods are usually used for disaster assessments over a wide area. The existing WSN solutions for real-time monitoring mainly transmit a small amount of specific sensor data through multi-hop paths based on the ZigBee technique, which has the weaknesses of limited communication capability and poor scalability. Furthermore, systems based on balloons and UAVs cannot continuously monitor a particular region in real time and may need the support of ground stations.

In view of the aforementioned issues, the main purpose of this paper is to develop a low-cost, low-complexity, and rapidly deployable WSN for rescue site monitoring after an earthquake. The hybrid WSN primarily consists of the monitoring center, wireless repeaters, monitor nodes, and sensor nodes. Specifically, a transmission control protocol (TCP)-based request-response scheme is implemented, such that the monitor nodes are capable of communicating with the monitoring center via wireless network. Moreover, the UDP-based image transmission algorithms with fast recovery are developed for real-time transmission of on-site monitor images. Furthermore, the specific implementation of the mechanical structure of the monitor node is conductive to easy portability, rapid deployment, and long-endurance missions. Furthermore, sensor nodes designed with small dimensions are used to monitor the environment by sensing different physical properties in narrow spaces. By building hybrid WSNs using those two types of nodes, the monitoring center can display real-time monitor images of the monitoring area and visualize all collected sensor data on GIS. The proposed system can be deployed on the areas with the highest probability of occurrences of secondary hazards after earthquakes. Thus, real-time environment monitoring of the localized rescue site can be achieved, which makes search and rescue activities much safer. To the authors' knowledge, this is the first real-time monitor system used in a post-earthquake rescue scene to provide rescuers with information that could highlight potential hazards to be avoided.

In the remainder of this paper, the system structure of the hybrid WSN is described in Sec. 2. The mechanical design and system configuration of two kinds of wireless nodes are elaborated in Sec. 3. Section 4 introduces the software architecture of our proposed system. Experimental results are further provided in Sec. 5. Finally, conclusions and future work are summarized in Sec. 6.

2 System Structure

As shown in Fig. 1, the hybrid WSN primarily consists of a monitoring center, wireless repeaters, multiple monitor nodes, and some sensor nodes.

The monitoring center first sends an IEEE802.11 signal toward the monitoring area via antenna and the repeaters are used to further cover the monitoring area. Notice that the emergency monitoring center set up temporarily at the earthquake disaster site can also send wireless

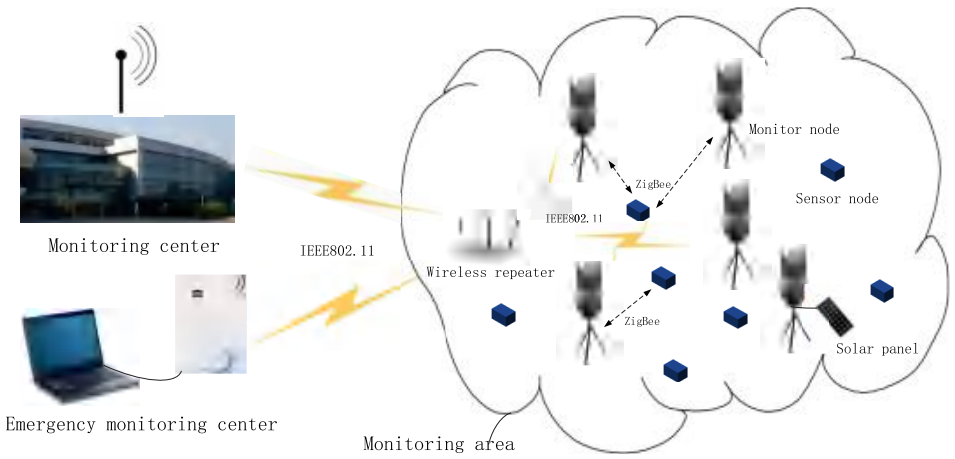

Fig. 1 System structure of the hybrid WSN.

signals using a directional route when power systems and communication systems are damaged due to earthquake shaking.

Monitor nodes are deployed on the monitoring area and sensor nodes can be scattered randomly around the monitor nodes. Specifically, the monitor node equipped with a high speed IEEE802.11-based wireless module can connect to the wireless local area network (WLAN) automatically when the wireless signal is detected. Thus the monitor nodes could transmit on-site monitor images captured by the CMOS camera and GPS-based geographical locations to the monitoring center via a wireless network. Furthermore, the large-capacity lithium batteries are installed inside the monitor node and the solar panels are optional for long-endurance missions. Additionally, each monitor node contains a ZigBee module used to communicate with the sensor nodes, which are designed with a small size to monitor the environment by sensing different physical properties, such as temperature, humidity, pressure, and vibration in narrow spaces. The collected sensor data are first passed to the monitor nodes and can be further transmitted to the monitoring center via wireless network. It should be mentioned that the positions of the sensor nodes can be estimated based on the received signal strength indicator (RSSI) values sent to the monitoring center along with the sensor data.

Finally, by building hybrid WSN using these two types of wireless nodes, the monitoring center can display real-time monitor images of the monitoring area and visualize all collected sensor data on GIS. Thus real-time environment monitoring is achieved.

3 Wireless Nodes Design

The hybrid WSN presented in this paper contains two kinds of wireless nodes, i.e., the monitor node and the sensor node. The design principles are first introduced in this section. Then the mechanism and the system configuration are detailed. Finally, we developed some prototypes based on the system design.

3.1 Monitor Node Design

It is apparent that the monitor node is a relatively complex device which implements many computationally demanding tasks such as image processing, position filtering, and wireless communications with other wireless nodes or the monitoring center.[28] Even though the monitor nodes are multifunctional devices, they should also have low-complexity, since the application requires many of them to be disassembled and reassembled in order to be portable and easily deployed in the rescue sites. Furthermore, they should have long-endurance performances in order to be able to operate for many hours while waiting for the rescue teams to complete the search and rescue missions. In addition, a waterproof and dustproof structure is also important for the purpose of surviving extreme weather conditions or other severe environments after earthquake disasters.

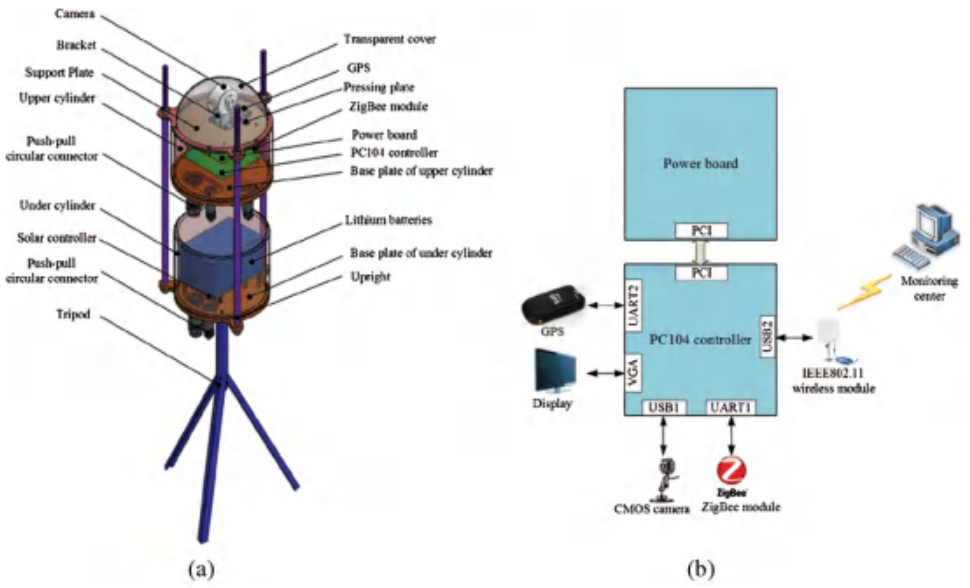

Fig. 2 The implementation of the monitor node. (a) Mechanical structure. (b) System configuration.

Taking all these into account, a monitor node is designed based on modular concepts. As shown in Fig. 2(a), the monitor node primarily contains two modules, including the upper cylinder and the under cylinder, which are mainly made of engineering plastics. Some functional components such as the PC104 controller, the CMOS camera, and the GPS are placed inside the upper cylinder. The peripheral devices (IEEE802.11 wireless module, and so on) are connected to the upper cylinder through waterproof push-pull circular connectors. On the other hand, large-capacity lithium batteries along with a solar controller are mounted inside the under cylinder. Two waterproof push-pull circular connectors, which are used to connect solar panels and power cables, respectively, are installed in the base plate of the under cylinder. Three uprights are used to support the upper cylinder above the under cylinder so that the whole monitor node has good static stability. A detachable tripod can be attached to the bottom of the monitor node, which is conductive to easy portability and rapid deployment. In particular, the design philosophy of modularity is incorporated into the design of the monitor node, which provides versatility for the monitor node and facilitates maintenance and future development of the monitor node, as new modules can easily be added to replace the obsolete modules.

The overview of the system configuration is introduced as seen in Fig. 2(b). The monitor node employs a PC104 module (Advantech 3363D) to control the whole system. A power board (Advantech 3910) connected to the PC104 controller with PCI interface to achieve the voltage transition and power transmission. A GPS (U-blox 6010) and a CMOS camera (Unifly 3900+) with resolution 640×480 pixels for capturing monitor images behind the monitor node are connected to the PC104 controller through USB ports. The ZigBee module is used to receive the sensor data sent from sensor nodes and record the RSSI values, which are further transmitted to the PC104 controller through the serial port with a baud rate of $115;200$ bits/s. Finally, all collected sensor data and monitor images are transmitted to the monitoring center through IEEE802.11 wireless module.

Based on the mechanism and system configuration introduced earlier, we developed several monitor node prototypes (see Fig. 3). The main technical parameters of the monitor node are tabulated in Table 1.

3.2 Sensor Node Design

The sensor node is a properly packaged device that collects information about the presence of people in a collapsed building space and the state of the ruins by sensing different physical properties such as sound and vibration and transmits them to the rescue teams. The information

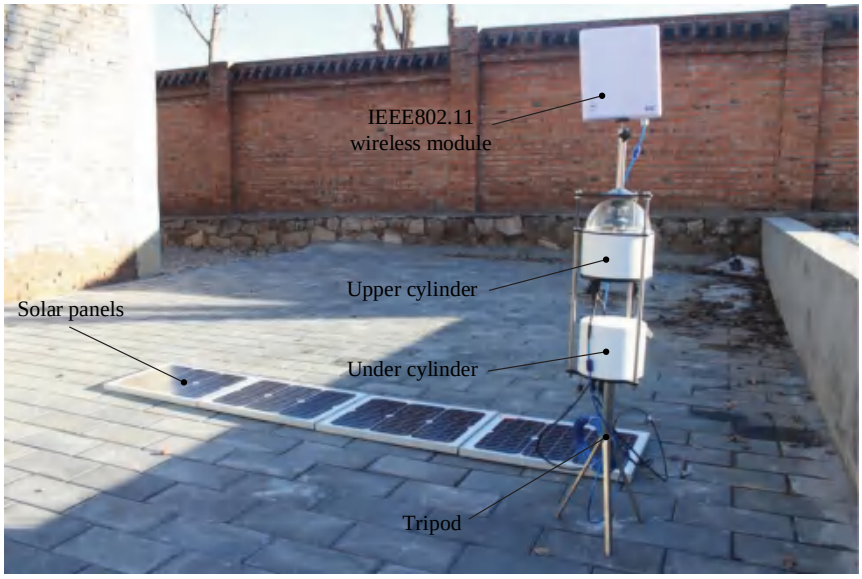

Fig. 3 The monitor node prototype.

Table 1 Technical parameters of the monitor node prototype.

Parameters	Value	Parameters	Value
Mass	6.5 kg	Camera frame rates	up to 60 fps
Diameter	165 mm	Camera resolution	640 × 480
Height without wireless card	819 mm	ZigBee data rate	200 Kps
Overall height	1197 mm	WLAN data rate	150 Mbps
ZigBee communication distance	20 m	Solar panels' power	100 W
WLAN communication distance	200 m	Power source	Lithium battery (11.1 V)

collected during the rescue operations is very valuable and helpful for the rescue teams to make the right decisions and complete their operations successfully. Specifically, the sensor node is designed with small size, such that we can easily deploy them in narrow spaces such as the crack of ruins. In addition, a ZigBee module installed on the sensor node facilitates the wireless communication with the monitor nodes by forming an ad-hoc sensor network.

Figure 4 shows the prototype and the system configuration of the sensor node. An Atmega128 microcontroller (STCl2C5A60S2) placed in a waterproof enclosure with dimensions

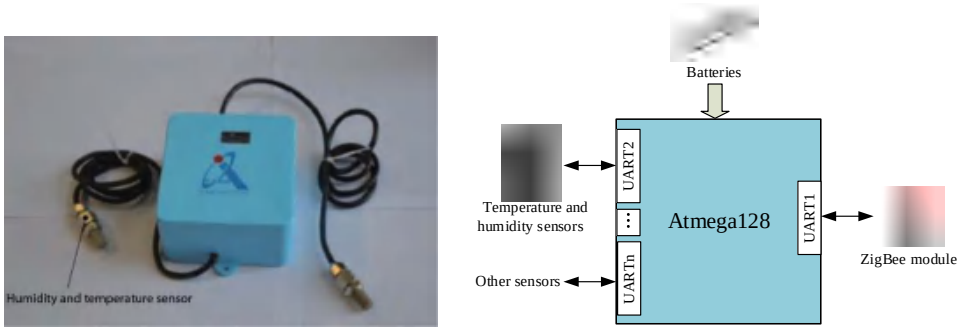

(a) (b)

Fig. 4 The design of the sensor node. (a) Prototype. (b) System configuration.

of 105 mm × 105 mm × 65 mm (length × width × depth) is used to control the sensors connected to the sensor node. A rechargeable lithium battery, which provides the power for the microcontroller and all the sensors, is mounted inside the enclosure. Notice that various sensors can be connected to the controller via serial ports, which is of primary importance for developments of application-specific sensor solutions quickly and cost effectively. The detailed description of the sensor node has been given in Ref. 29. Thus it is omitted. In this study, a SHT-10-based soil sensor is used to collect temperature and relative humidity data around the sensor node.

4 Software Architecture

High attenuation, the mobility of wireless nodes, and the movement of obstacles and machinery in the rescue sites can result in significant change of the communication quality in the network at unpredictable times and rates.[30–32] Therefore, a robust communication based on a client-server model has been implemented using a request-response scheme. This scheme uses TCP sockets to support reliable communication among the monitor nodes and the monitoring center. In addition, a reconnection mechanism is developed in order to maintain strong connectivity. In order to facilitate the localization of the sensor node, a distance estimation method has been implemented. In order to meet the requirements of in-time delivery of on-site monitor images, UDP-based image transmission algorithms with fast recovery have been developed.

4.1 TCP-Based Request-Response Scheme

The basic architecture of the request-response scheme is shown in Fig. 5. The system is based on client-server model, in which the monitor nodes act as servers while the monitoring center serves as client. In addition, TCP is used such that it allows reliable, ordered, and error-checked delivery of a stream of octets between both sides. In particular, the client connects to the server and then requests data such as GPS locations, sensor data, RSSI values, and monitor images. After receiving a request, the server creates a response and sends the corresponding data to the client. Specially, requests and sensor data of small size are transferred via TCP, while the monitor images are split into chunks of a certain size and UDP-based data transfer is used to meet the requirement of real-time network transmission. When receiving the data sent from the monitor node via TCP, the monitoring center first stores the collected data in Microsoft SQL Server database and then visualizes all sensor data on GIS. Meanwhile, a reconnection mechanism is developed for the client to reconnect to the server when the network connection is suddenly broken. In detail, after sending the TCP request, we can consider the TCP connection to be broken if the response is not retrieved within a period of time. Then the client would automatically attempt to reconnect to the server at set intervals until it continues to fail after a certain number of requests.

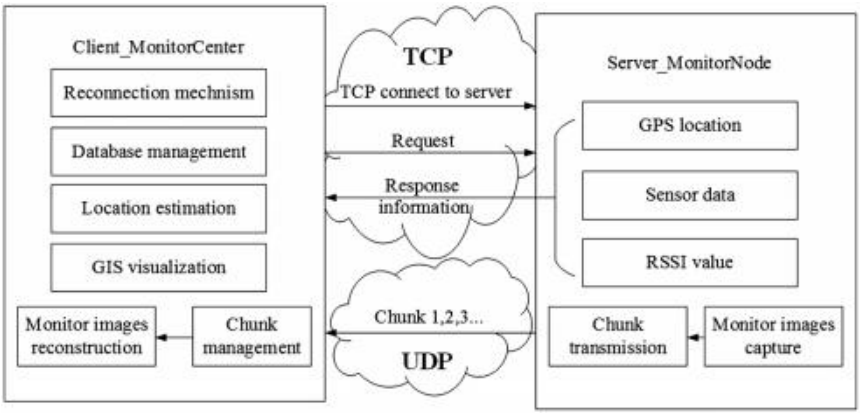

Fig. 5 The request-response scheme.

4.2 Localization of the Sensor Node

The positions of the sensor nodes can be estimated based on the RSSI values sent to the monitoring center along with the sensor data. In this study, the lognormal shadowing model expressed by Eq. (1) is used to convert the signal strength into distance.[33]

$$\mathrm{PL}(d) = \mathrm{PL}_c + 10\beta \log \frac{d}{d_0} + X(\sigma); \tag{1}$$

where β is the path loss exponent that characterizes how fast the path loss increases with increasing distance d, and $X(\sigma)$ is a zero-mean Gaussian random variable with a standard deviation σ. $\mathrm{PL}(d)$ and PL_c are the RSSI values at the distance d and the reference distance d_0, respectively. Notice that the RSSI value is highly influenced by environmental factors, the calibration of the parameters of the lognormal shadowing model has been prematurely completed, where the RSSI values and distances are evaluated in a controlled environment. It should be mentioned that the monitoring center can further compute the positions of the sensor nodes using methods such as trilateration[34] or bounding box[35] when enough information about distances are acquired.

4.3 Image Transmission

In networks with small round trip times (RTTs), the request-response and the single TCP approach are able to cope with packet loss via retransmissions. With increasing delay and packet loss, the single TCP approach deteriorates rapidly, while the impact of the request-response system is limited. Compared with TCP, UDP is simpler and accommodates less information allowing link data multiplexing, which is conductive to rapid image transmission. For these reasons, a UDP-based application protocol has been designed to achieve an acceptable tradeoff between transmission speed and packet loss for image transmission, which is beneficial in the case of bad network conditions such as on an earthquake site.

In detail, when the transmission-start instruction is given, the image transmission procedure of the monitor node is executed as illustrated in Algorithm 1. Specifically, r indicates the compression ratio of the image frame, which can be set manually. In low-latency networks, image quality is able to be improved by decreasing the compression ratio. In congested networks, however, a low compression ratio is used to guarantee the real-time image transmission. It should be noticed that this value cannot be adjusted automatically based on network conditions at present, which has to be improved in the future. Notice also that compared with interframe compression method, where the current frame is compressed using one or more earlier or later frames in a sequence, we only use the current frame to compress the image frame, considering that when packet loss of a frame occurs, it does not affect other frames, which is conductive to fast recovery in the delivery of monitor images.

In image transmission, every compressed frame is split into chunks of size L_{total} bytes. As reported in Fig. 6, chunks from the monitor node to the monitor center have the following fields.

1. Category: Type of chunk ("F," "M," and "L" represent first, middle, and last chunk of the image frame, respectively). This field is useful in synthesis of a plurality of chunks into an image frame.
2. FrameSize: Number of bytes of the compressed frame. Denote this value by L_{frame}.
3. ChunkNumber: The N_{chunk}'th chunk of the current frame.
4. UsedPayloadSize: Length of the following valid data. Let this value be L_{usedsize}.
5. Payload: Data of the image frame.

It is obvious that $L_{\mathrm{total}} = 4 \times 4 + L_{\mathrm{payload}}$. Notice that after sending L_{total} bytes of data via UDP, the monitor node should wait for a delay of T_{interval} ms and then send next chunk to guarantee the stability of image transmission. In order to maximize the in-order throughput, a tradeoff between chunk size L_{payload} and time interval T_{interval} has to be found. The experiments show that when $L_{\mathrm{payload}} = 1024$ bytes and $T_{\mathrm{interval}} = 1$ ms, the packet loss and delay can be significantly reduced.

In the monitor center (i.e., TCP client), the chunks are retrieved via UDP according to their order within the queue. Algorithm 2 shows the details about the images' reconstruction process. After fetching a chunk, the judgment of the category of this chunk is implemented first. If it is the first chunk of the image frame, new L_{frame} bytes buffer and copy the data in the payload into the

Algorithm 1 Image transmission of the monitor node.

1: repeat
2: Image capture.
3: Image compression at ratio r.
4: New L_{total} bytes of send buffer, set the L_{frame} value, n_{chunk} ¼ 0.
5: while (1) do
6: n_{chunk} þ þ.
7: Try to read $L_{payload}$ bytes of data into the send buffer.
8: if (The actual number of bytes read into the buffer is small than $L_{payload}$) then
9: category = "L" $L_{usedsize}$ ¼ L_{read}, send L_{total} bytes of data via UDP.
10: Break.
11: else
12: (n_{chunk} ¼¼ 1) ? category = "F":category = "M."
13: $L_{usedsize}$ ¼ $L_{payload}$, send L_{total} bytes of data via UDP.
14: end if
15: Sleep ($T_{interval}$).
16: end while
17: until stop transmission

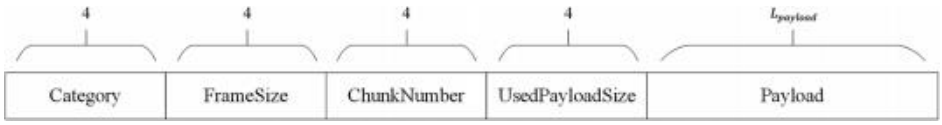

Fig. 6 Proposed protocol of chunks. Length, expressed in bytes, is indicated for each field.

buffer. If the chunk belongs to middle chunks of the image frame, copy the image data into the corresponding buffer, i.e., $L_{payload}$ bytes of buffer whose start address is &buffer [ðn$_{chunk}$ − 1þ × $L_{payload}$]. Otherwise, determine if the number of bytes received $L_{receive}$ is equal to the actual number of bytes of the image frame. If $L_{receive}$ ¼ L_{frame}, save and display the current frame, otherwise, discard this frame due to packet loss.

The proposed image transmission scheme uses UDP and features low-complexity on both server and client, resulting in in-time delivery of the monitor images and high scalability. It allows parallel data transmission of multiple servers (namely, multiple monitor nodes) by constructing multiple UDP streams. In addition, intraframe compression is used instead of interframe compression, which facilitates the fast recovery in the delivery of the monitor images.

5 Experiments

In order to illustrate the feasibility and effectiveness of the proposed monitor system, a field experiment was performed at the Training Base of Emergency Seismic Rescue Troops of China. The photograph of the test site is shown in Fig. 7. In this picture, the monitoring center is near the left of center and the monitoring area is in the right-most. Specially, the two places are about 200 m apart. A wireless virtual private network (VPN) gigabit router (TP-LINK TL-ER604W) is used to spread the IEEE802.11 signal sent from the monitor center via the antenna to cover the monitoring area. The average RTT is about 10 ms to several tens ms.

Algorithm 2 Image reconstruction of the monitor center.

1: repeat
2: Fetch the chunk.
3: if (category == "F") then
4: $L_{receive} = 0$, $L_{receive} = L_{payload}$.
5: New L_{frame} bytes of buffer.
6: Copy $L_{payload}$ bytes from payload to buffer.
7: else if (category == "M") then
8: Copy $L_{payload}$ bytes from payload to &buffer [$n_{chunk} - 1 \times L_{payload}$].
9: $L_{receive} = L_{payload}$.
10: else
11: Copy $L_{usedsize}$ bytes from payload to &buffer [$n_{chunk} - 1 \times L_{payload}$].
12: $L_{receive} = L_{usedsize}$.
13: if ($L_{receive} == L_{frame}$) then
14: Save the frame.
15: Display the frame.
16: end if
17: end if
18: until stop transmission

Fig. 7 Photograph of the field test site at the Training Base of Emergency Seismic Rescue Troops of China. The monitoring center is located near the left of the center and the monitoring area is just at the right of the center.

Moreover, as shown in Fig. 8, six monitor nodes, four of which were connected to solar panels, and six sensor nodes were deployed in the monitoring area to organize into a mesh network.

In the experiment, a rescue robot controlled by a remote control was placed in the view of some monitor nodes. The robot is able to go forward/backward, turn left/right on the ground.

Fig. 8 Photograph of the field test arrangement. Six monitor nodes and six sensor nodes are deployed in the monitoring area and a rescue robot is placed in near the lower right of center.

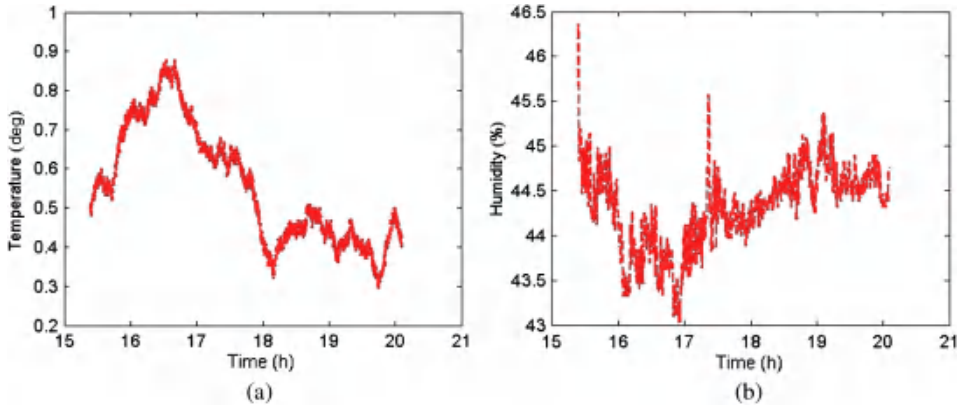

Fig. 9 Received sensor information. (a) Temperature. (b) Humidity.

Then we started all wireless nodes and the environment monitoring started. Figure 9 shows the time evolutions of the temperature and humidity acquired by the sensor node 3. Specifically, the receiving frequency was 1 Hz and 5 h of data between about 15:00 and 20:00 were recorded. These sensor data were further displayed graphically on GIS as shown in Fig. 10 along with the received GPS data. Notice that the first and the sixth monitor nodes were placed in the indoor environment and were unable to be located using GPS, such that the data of these two nodes were not shown. The experimental results verify the robustness and effectiveness of the ZigBee communication between the sensor nodes and the monitor nodes and the TCP-based request-response scheme.

In order to further evaluate the performance of our proposed system, we let the rescue robot move through the monitoring area. Figure 11 shows the monitoring results at the monitoring center, in which the image series were obtained at a frame rate of about 10 frames per second (fps) and at a compression ratio of 5%. It can be concluded that the hybrid WSN realizes stable, to some extent, image transmission of parallel multichannels and could display the monitor images on the monitor with acceptable time delays. Furthermore, define frame error rate (FER) as the relationship between the number of frames sent by the monitor node N_{sed} and the number of frames received by the monitoring center N_{rec}, taking the form

$$\mathrm{FER} = \frac{N_{sed} - N_{rec}}{N_{sed}}. \tag{2}$$

The FER of each monitor node within about half an hour is shown in Table 2. It is observed that the maximum FER is less than 4%, which is an acceptable result in this network condition.

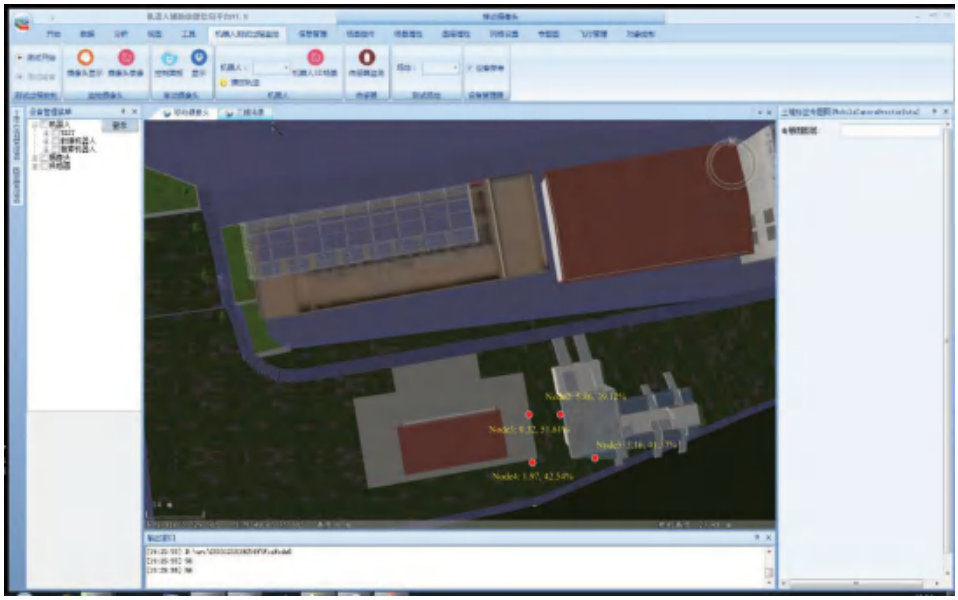

Fig. 10 A screen shot of the GIS. Red dots represent the location of monitor nodes, and yellow number represents the sensor information sent to the monitoring center through this monitor node.

Fig. 11 Video clip of the monitoring result in the field experiment (Video 1 MPEG, 11.1 MB) [URL: http://dx.doi.org/10.1117/1.JRS.10.036020.1].

Table 2 FER of each monitor node.

Node 1	Node 2	Node 3	Node 4	Node 5	Node 6
2.9%	3.9%	3.6%	3.6%	1.8%	3.3%

6 Conclusion and Future Work

In this paper, a WSN for rescue site monitoring after earthquake has been developed, which contains two kinds of wireless nodes, i.e., the monitor node and the sensor node. In particular, the monitor node equipped with IEEE802.11 wireless module is capable of transmitting on-site monitor images and GPS-based geographical locations to the monitoring center via wireless network. In addition, a detachable tripod and solar panels can be attached to the monitor node,

which are conductive to easy portability, rapid deployment, and long-endurance missions. Sensor nodes are designed with small dimensions to monitor the environment by sensing different physical properties, such as temperature, humidity, pressure, and vibration in narrow spaces. Additionally, the collected sensor data are first sent to the monitor nodes based on ZigBee technique and are further transmitted to the monitoring center along with the monitor images. Physical experiments have been conducted and the experimental results demonstrate that the monitoring center can display immediate monitor images of the monitoring area and visualize all collected sensor data on GIS by building WSN using these wireless nodes.

The ongoing research will seek to implement some intelligent monitoring algorithms (e.g., object recognition or intrusion detection) on the monitor node for a better monitoring performance. Other work will focus on optimizing the mechanical design of the monitor node (e.g., miniaturization or light weight) and the localization algorithm of the sensor node. Our final aim is naturally to achieve future applications of the proposed WSN for rescue site monitoring after earthquake.

Acknowledgments

This work was supported in part by the National Natural Science Foundation of China under Grant Nos. 61233014, 61333016, and 51175496, in part by the Foundation for Innovative Research Groups of the National Natural Science Foundation of China under Grant No. 61421004, in part by the Beijing Natural Science Foundation under Grant No. 3141002, and in part by the National Key Technology Research and Development Program of China under Grant No. 2014BAK12B03-02.

References

1. R. D. Kearns et al., "Disasters; the 2010 Haitian earthquake and the evacuation of burn victims to US burn centers," Burns 40(6), 1121–1132 (2014).
2. Q. Yao and Z. Qiang, "Thermal infrared anomaly indicating unformed strong earthquake sequences," J. Appl. Remote Sens. 9(1), 096089 (2015).
3. K. Smith, Environmental Hazards: Assessing Risk and Reducing Disaster, Taylor & Francis Group, Routledge (2013).
4. S. Ploeger et al., "Development of the CanRisk earthquake injury model," Nat. Hazards 80(2), 1171–1194 (2016).
5. J. Daniell et al., "The value of life in earthquakes and other natural disasters: historical costs and the benefits of investing in life safety," in Proc. of the Tenth Pacific Conf. on Earthquake Engineering, pp. 6–8 (2015).
6. P. Gamba and F. Casciati, "GIS and image understanding for near-real-time earthquake damage assessment," Photogramm. Eng. Remote Sens. 64(10), 987–994 (1998).
7. F. Mantovani, R. Soeters, and C. V. Westen, "Remote sensing techniques for landslide studies and hazard zonation in Europe," Geomorphology 15(3), 213–225 (1996).
8. M. Moretti, L. Margheriti, and A. Govoni, "Rapid response to the earthquake emergencies in Italy: temporary seismic networks coordinated deployments in the last five years," in Earthquakes and Their Impact on Society, pp. 585–599, Springer, New York City (2016).
9. J. Bingli, Z. Yimei, and T. Muqile, "Dynamic plotting system of earthquake emergency response in wisdom city," in Proc. of the Sixth Int. Conf. on Measuring Technology and Mechatronics Automation, pp. 271–274, IEEE (2014).
10. S. Liang et al., "Design of an early-warning system based on wireless sensor network for landslide," Chin. J. Sens. Actuators 23(8), 1184–1188 (2010).
11. D. M. Tralli et al., "Satellite remote sensing of earthquake, volcano, flood, landslide and coastal inundation hazards," ISPRS J. Photogramm. Remote Sens. 59(4), 185–198 (2005).
12. M. Schmidt and C. Witte, "Monitoring aquatic weeds in a river system using SPOT 5 satellite imagery," J. Appl. Remote Sens. 4(1), 043528 (2010).
13. N. Minamiguchi, "The application of geospatial and disaster information for food insecurity and agricultural drought monitoring and assessment by the FAO GIEWS and Asia

FIVIMS," in Workshop on Reducing Food Insecurity Associated with Natural Disasters in Asia and the Pacific, Vol. 27, p. 28 (2005).
14. N. Pettorelli, K. Safi, and W. Turner, "Satellite remote sensing, biodiversity research and conservation of the future," Philos. Trans. R. Soc., B: Biol. Sci. 369(1643), 20130190 (2014).
15. D. Chen et al., "Natural disaster monitoring with wireless sensor networks: a case study of data-intensive applications upon low-cost scalable systems," Mobile Networks Appl. 18(5), 651–663 (2013).
16. N. Ahmad et al., "Flood prediction and disaster risk analysis using GIS based wireless sensor networks, a review," J. Basic Appl. Sci. Res. 3(8), 632–643 (2013).
17. T. Arampatzis, J. Lygeros, and S. Manesis, "A survey of applications of wireless sensors and wireless sensor networks," in Proc. of the Mediterrean Conf. on Control and Automation, pp. 719–724, IEEE (2005).
18. N. Pogkas et al., "Architecture design and implementation of an ad-hoc network for disaster relief operations," IEEE Trans. Ind. Inf. 3(1), 63–72 (2007).
19. R. Ohbayashi et al., "Monitoring system for landslide disaster by wireless sensing node network," in Proc. of the SICE Annual Conf., pp. 1704–1710, IEEE (2008).
20. J. Q. Huang et al., "Development and test of aquacultural water quality monitoring system based on wireless sensor network," Trans. Chin. Soc. Agric. Eng. 29(4), 183–190 (2013).
21. K. Kawamura et al., "Mapping herbage biomass and nitrogen status in an Italian ryegrass (Lolium multiflorum L.) field using a digital video camera with balloon system," J. Appl. Remote Sens. 5(1), 053562 (2011).
22. J. A. Shaw et al., "Multispectral imaging systems on tethered balloons for optical remote sensing education and research," J. Appl. Remote Sens. 6(1), 063613 (2012).
23. S. M. Adams and C. J. Friedland, "A survey of unmanned aerial vehicle (UAV) usage for imagery collection in disaster research and management," in Int. Workshop on Remote Sensing for Disaster Response (2011).
24. S. Rathinam et al., "Vision-based monitoring of locally linear structures using an unmanned aerial vehicle," J. Infrastruct. Syst. 14(1), 52–63 (2008).
25. D. Asahizawa et al., "Disaster surveillance video transmission system by wireless ballooned network," in Proc. of the Int. Conf. on Advanced Information Networking and Applications Workshops, pp. 884–889 (2009).
26. Z. Li, F. Yang, and W. Wang, "Study on the evaluation of UAV disaster monitoring system architecture based on the RSBFNN algorithmic method," Appl. Math. Inf. Sci. 9(3), 1455–1465 (2015).
27. N. M. Figueira et al., "Mission-oriented sensor arrays and uavs-a case study on environmental monitoring," Int. Arch. Photogramm. Remote Sens. Spatial Inf. Sci. XL-1/W4(1), 305–312 (2015).
28. L. Gasparini et al., "An ultralow-power wireless camera node: development and performance analysis," IEEE Trans. Instrum. Meas. 60(12), 3824–3832 (2011).
29. H. Chang et al., "A new agriculture monitoring system based on WSNs," in Proc. of the Int. Conf. on Signal Processing, pp. 1755–1760, IEEE (2014).
30. M. M. U. Rathore et al., "Real-time big data analytical architecture for remote sensing application," IEEE J. Sel. Top. Appl. Earth Obs. Remote Sens. 8(10), 4610–4621 (2015).
31. L. Liu, S. Zhou, and J. H. Cui, "Prospects and problems of wireless communication for underwater sensor networks," Wirel. Commun. Mob. Comput. 8(8), 977–994 (2008).
32. I. F. Akyildiz, Z. Sun, and M. C. Vuran, "Signal propagation techniques for wireless underground communication networks," Phys. Commun. 2(3), 167–183 (2009).
33. G. Durgin, T. S. Rappaport, and H. Xu, "Measurements and models for radio path loss and penetration loss in and around homes and trees at 5.85 GHz," IEEE Trans. Commun. 46(11), 1484–1496 (1998).
34. A. Boukerche et al., "Localization systems for wireless sensor networks," IEEE Wireless Commun. 14(6), 6–12 (2007).
35. S. Simic and S. Sastry, "Distributed localization in wireless ad hoc networks," Technical Report UCB/ERL M02/26, University of California, Berkeley, California (2002).

Rui Wang received his BE in automation from Beijing Institute of Technology, China, in July 2013. He is currently working toward his PhD in control theory and control engineering at the State Key Laboratory of Management and Control for Complex Systems, Institute of Automation, Chinese Academy of Sciences. He is also with the University of Chinese Academy of Sciences, Beijing. His research interests include wireless sensor networks, intelligent control, and biomimetic robots.

Shuo Wang received his ME degree in industrial automation from Northeastern University, Shenyang, and his PhD in control theory and control engineering from the Institute of Automation, Chinese Academy of Sciences, Beijing, China, in 1995, 1998, and 2001, respectively. He is currently a professor in the State Key Laboratory of Management and Control for Complex Systems, Institute of Automation, Chinese Academy of Sciences. His research interests include biomimetic robots, underwater robots, and multirobot systems.

Chong Tang received his BE from Northwestern Polytechnical University, China, in July 2014. He is currently working toward his PhD in control theory and control engineering at the State Key Laboratory of Management and Control for Complex Systems, Institute of Automation, Chinese Academy of Sciences. His research interests include intelligent control, robotics, and biomimetic robots.

Xiaoguang Zhao received her ME and PhD degrees in control theory and control engineering from the Shenyang Institute of Automation, Chinese Academy of Sciences, in 1998 and 2001, respectively. She is currently a professor in the State Key Laboratory of Management and Control for Complex Systems, Institute of Automation, the Chinese Academy of Sciences. Her research interests include intelligent robots, robot vision, and wireless sensor networks.

Weijian Hu received his ME from Dalian University of Technology in 1999. He is currently a senior engineer in the National Earthquake Response Support Service. His research interests include earthquake relief technology and rescue equipments.

Min Tan received his BE from Tsinghua University, and his PhD in control theory and control engineering from the Institute of Automation, Chinese Academy of Sciences, Beijing, China, in 1986 and 1990, respectively. He is currently a professor in the State Key Laboratory of Management and Control for Complex Systems, Institute of Automation, Chinese Academy of Sciences. His research interests include advanced robot control, biomimetic robots, and multirobot systems.

Bowei Gao received his BE degree from University of Science and Technology Beijing, in 2011. He is currently an engineer in the National Earthquake Response Support Service. His research interests include earthquake relief technology and rescue equipments.